Egyptian Journal of Chemistry

http://ejchem.journals.ekb.eg/

Functionalization of Magnetic-Chitosan Nanocomposite for Enhancing Th(IV) Ions Sorption

Said I. Mohamady

Uranium ore processing department, Production sector, Nuclear Materials Authority, P.O Box 530, El-Maadi, Cairo, Egypt

DESIGNING new chelating sorbents for the sorption of thorium as (Th^{4+}) has become an impending challenge. This study describes a simple one-pot in situ co-precipitation method was used to synthesize a multifunctional magnetic-chitosan nanocomposite core-shell for enhanced Th^{4+} ions sorption from aqueous solutions. The synthesized biosorbent was well characterized by various techniques such as FTIR, XRD, pH_{zpc}, TEM, VSM and elemental analysis. The sorption behavior of magnetic-chitosan nanocomposite (R-I) is systematically compared to the performance of functionalized magnetic-chitosan nanocomposite (R-II). The magnetic nanocomposite sizes around 25.0 nm. The grafting of methylene phosphonic groups on chitosan increased Th^{4+} sorption efficiency. Maximum sorption capacities reach 89.7 and 142.3 mg Th g^{-1} for R-I, and R-II sorbents, respectively at pH 3.5. Kinetics, isotherms, and thermodynamic behaviors of Th^{4+} ions sorption into the synthesized nanocomposite from an aqueous solution were studied in detail. The studies showed that the Langmuir isotherm and pseudo-second order model gave a better description for the sorption process. The sorption is spontaneous, endothermic and controlled by entropic change. EDTA solutions (0.25 M) can be efficiently used for metal recovery and sorbent can be recycled for at least 5 cycles without significant loss in sorption/desorption performances.

Keywords: Magnetic-chitosan; iminodiphosphonic acid; phosphomethylation; nanocomposite; Thorium(IV); isotherms; desorption; sorbent recycling.

Introduction

Thorium is considered the most important element for nuclear energy production; its resources are rather limited and the expected shortage in the near future. Moreover, it is one of the most hazardous biotoxic radionuclides. Therefore, separation and recovery of thorium is a significance process not only for reasonable utilization of thorium resources but also for environmental protection [1-5]. Thorium (Th^{4+}) is one of the major radioactive ions that is very useful as a nuclear fuel which can be used as nuclear fuel by conversion into uranium-233 (^{232}U). Soil, rocks, sand and water are the main source of thorium and because its availability is 3–4 times higher than uranium, this ion has attracted a lot of interest as a nuclear fuel. Furthermore, in the cycle of using thorium as the primary fuel, the raw material is less used and consequently, the waste produced is less too.

In addition to nuclear power plants and manufacture of nuclear weapons applications, thorium have been extensively used in varieties of industrial applications such as: high-quality lenses sinker bars, the electron microscope, glass and pottery glaze, ceramics, lantern mantles, welding rods and laboratory crucibles. Thorium is one of the radionuclides and the main nuclear for energy production exhibits dangerous problems to the environment through activities including mining, milling, and spent nuclear reprocessing. These processes create radioactive wastes which cause acute toxicological effects for human including lung cancer, pancreatic cancer, and liver disease..etc.[1-8].

Sorption processes through ion-exchange or chelation interaction represents a fundamental and impressive technique for metal ions removal from aqueous solutions; owing to its simplicity, good selectivity, low cost, applicability, fast kinetics, ecofriendly and highly efficient. Different sorbents such as metal oxides, activated carbons, resins, impregnated resins, metal-organic frameworks (MOFs), nanocomposites and biosorbents have been reported for thorium sorption [1,3,4]. Chelating or coordinating resins that bear one or more donor atoms may thus represent interesting materials for binding metal ions. In chelating sorbents, the most frequently used donor atoms containing functional groups are nitrogen (i.e., amines, azo groups, amides, and nitriles groups), oxygen (i.e., carboxylic, hydroxyl, phenolic, ether, and carbonyl groups), phosphorous (i.e., phosphonate and phosphoryl groups), and sulfur (i.e., thiols, thiocarbamates, and thio-ethers groups). Grafting new and multi-functional groups with different heteroatoms on polymer surface could increase active sites density for metal complexing as well as enhancing selectivity and sorption capacity, over a wide range of pH [7-12]. The choice of chelating moieties is usually based on the affinity of the reactive groups to the target metal ions according the Hard-Soft/Acid-Base theory (HSAB). The HSAB defined by Pearson [13]: hard acids (low polarizability and high electronegativity) prefer to associate with hard bases (N, O, F), while soft acids (high polarizability and low electronegativity) prefer to associate with soft bases (P, S, I).Thorium ions (Th^{4+}) behaves as a hard acid showing great reactivity toward hard bases. Hence,

chelating agents, having functional groups of P, N, and O, exhibit higher efficiency toward selective sorption of thorium (i.e. high sorption capacity with selective separation properties). Organophosphorus compounds and their derivatives are also known as good metal-complexing agents for various metal ions especially for thorium and uranium [9-18].

In the last decades numerous studies on metal biosorption have been inspired by the ion-exchange and chelating systems for mimicking conventional resins using biomass that bear similar reactive groups for metal recovery from dilute solutions. These renewable resources are usually cost effective, abundant and they can be used as produced or chemically modified for improving sorption performance. Chitosan, an amino-polysaccharide produced from crustacean shells. However, these materials have relatively low sorption capacities for metal ions and it is generally necessary grafting specific functional groups on their polymer backbone or incorporating other ion-exchanger for reaching significant sorption capacities [16, 17].

Global sorption properties are not only controlled by the proper reactivity of functional groups but also by the mass transfer properties of the resins: textural properties (i.e. porosity and specific surface area) control the accessibility to internal reactive groups. Improving these criteria may consist in decreasing the size of sorbent particles to decrease the intraparticle diffusion path. The main drawback at using micro or nano-objects consists of the management of separation and confinement properties. This drawback can be overcome using magnetic micro/nano-particles [16-21].

Nanocomposite is a multiphase material, for which one of them has nano-sized dimensions, especially magnetic-nanocomposites embedded with Fe$_3$O$_4$ nanoparticles, received a great attention since decreasing the particles sizes allows substantially reducing the limitations due to resistance to intraparticle diffusion and increasing specific surface area. Moreover, an external magnetic field can be used for recovering spent sorbents at the end of the sorption process [17-21]. Thus, a direct reaction is described to prepare hydrophobic α-aminomethylphosphonic acid as new magnetic-chitosan-nanocomposites (R-II). This sorbent was

characterized by CHNP analysis, FTIR, pH_{ZPC}, TEM, XRD, and VSM. The sorption properties of prepared functionalized magnetic-chitosan nanocomposites (R-II) have been compared to those of raw magnetic-chitosan nanocomposites (R-I) for thorium (Th^{4+}) ions: through the study of pH effect, uptake kinetics, sorption isotherms, and thermodynamic parameters. Regeneration and recycling of the sorbents were investigated for five cycles.

Materials and Methods

Materials

Chitosan (CAS: 9012-76-4) were supplied by Acros Organics (USA), dimethyl-formamide (DMF), and $FeSO_4·7H_2O$ and $FeCl_3$ were purchased from Wako Chemical Co. Ltd., Japan. Arsenazo III, formaldehyde solution (HCHO, 37%) and phosphorous acid were obtained from Fluka. Thorium stock solution was prepared by dissolving thorium sulphate ($Th(SO_4)_2.8H_2O$, Sigma–Aldrich) in conc. H_2SO_4 under heating before being diluted in demineralized water to a final concentration: 1.0 g Th L^{-1}. Thorium concentration was determined using Arsenazo III colorimetric method [18] and spectrophotometer (Metertech Inc, model SP-8001).

Sorbent synthesis: functionalization of magnetic-chitosan nanocomposite

Phosphorous acid (2.5 g) was dissolved in 75 mL of H_2O and HCl (1:1, v/v). After addition of Chitosan (CS: 2 g), the mixture was heated to reflux in a 200mL three-necked flask (with thermometer, condenser, and dropping funnel) and formaldehyde solution (20mL) was added dropwise for 1h. The mixture was stirred (150 rpm) and kept at reflux for 24 additional hours. The final product polyaminophosphonic acid-functionalized chitosan [19, 20]. After reaction complete, a mixture of Fe^{II}/Fe^{III} (1:2 molar ratio corresponding to $FeCl_2·4H_2O$ (1.21g) and $FeCl_3$ (1.94 g), respectively, for an initial amount of chitosan (2 g)), and then the reaction mixture was allowed to complete homogeneity distribution. Then, the solution was chemically precipitated at 40°C by adding NaOH (10 M) dropwise with constant stirring under the protection of Ar gas at controlled pH:10.0−10.5. The reaction mixture was stirred (800 rpm) for another 12 hours. The suspension was hydrothermal treatment at 90 °C for 1h under continuous stirring, before being separated by decantation and magnetic attraction. The precipitate was extensively washed with distilled water and ethanol, each time followed by centrifugation until the supernatant had a neutral pH. Finally, the final product was dried at 40 ºC for 24 hours. Secondly, magnetic chitosan nanocomposites (R-I) were synthesized by the same procedure and weight) with raw chitosan as the precursor (instead of polyaminophosphonic-functionalized chitosan), followed by hydrothermal treatment, is reported elsewhere [17, 21].

Characterization of materials

The elemental analysis was performed on a Micro Corder JM10 (Japan). The FTIR spectra were obtained by a JASCO-FT-IR-6600 spectrometer, Japan. X-ray diffraction (XRD) patterns were obtained at room temperature using a Smart Lab X-Ray Diffractometer (RIGAKU, Japan). The magnetic properties were measured on a vibrating sample magnetometer (VSM) (730T, Lakeshoper, America) at room temperature. The dimension and morphology of sorbent particles were observed by transmission electron microscope-TEM (JEOL-2100, Japan) at the Micro Analytical Unit (Menoufia University, Egypt).

Sorption and desorption experiments

Batch experiments were carried out by mixing of 10 mg of sorbent with 20 mL of aqueous Th^{4+}solution (i.e., C_o: 50 mg Th L^{-1}) in 30 mL glass bottles. The sorption experiments were agitated and performed at 200 rpm at room temperature (i.e., 25 ±1ºC) for 2 h. After equilibration and phase separation (by filtration through 1.2 μm pore-size filter membrane and magnetic separation).The Th^{4+} ion concentrations before and after the sorption were determined. The sorption capacity (q_{eq}, mg ThL^{-1}) was calculated according to mass balance equation: $q_{eq} = (C_o-C_{eq})V/m$. where, C_o and C_{eq}, (mg ThL^{-1}), are the initial and final Th^{4+}concentration, respectively. m (g) is the weight of sorbent and V (L) is volume of aqueous metal solution. For the sorption isotherm experiments, the initial pH was 3.5, while the initial Th^{4+} concentration varied from 25 and 300 mg L^{-1} at room temperature. Kinetic measurements were performed by varying contact times for a sorbent dose 0.5 g/L. Urea and EDTA (0.25 M) were chosen as the eluent for the study of metal desorption. The

contact time between the eluent and the metal-loaded sorbent was set to 30 min. The sorption yield after regeneration for five cycles was compared to the value reached for the first cycle.

Modeling of uptake kinetics and sorption isotherms
Modeling of uptake kinetics

Several kinetic models are needed to examine the sorption mechanism from a liquid phase and to interpret the experimental data. Pseudo-first-order rate equation (PFORE) and pseudo-second-order rate equation (PSORE) are used to explain the kinetics of sorption to investigate the sorption mechanism [15-17, 21].

PFORE assumes that the rate of change of solute uptake with time is directly proportional to the difference in saturation concentration and the amount of solid uptake to time, while PSORE is based on the assumption that the biosorption follows chemisorptions mechanism and predicts the behavior over the whole range of concentration and is in agreement with biosorption mechanism being the controlling step rate [15-17].The linear forms of PFORE, PSORE, and the simplified model of resistance to intraparticle diffusion (sRIDE, the so-called Weber and Morris model, Eq. (3)) are reported in Eqs. (1) (2), and (3) respectively:

$$\log (q_e - q_t) = \log q_e - \frac{k_1}{2.303} t \qquad \text{Eq. (1)}$$

$$\frac{t}{q_t} = \frac{1}{k_2 q_e^2} + \frac{1}{q_e} t \qquad \text{Eq. (2)}$$

$$q_t = k_{int}. t^{1/2} + C \qquad \text{Eq. (3)}$$

Where, q_e and q_t (mg g^{-1}) are the sorption capacities at equilibrium and time t (min), respectively.k_1 is the rate constant of PFORE (min^{-1}), k_2 (g mg^{-1} min^{-1}) is the rate constant of PSORE, k_{int} (mg g^{-1} min$^{-0.5}$) is the sRIDE coefficient, and C is a parameter related to the thickness of the film surrounding the particle (should tend to 0 if the contribution of resistance to film diffusion is negligible).

Modeling of sorption isotherms

The sorption equilibrium data have been analyzed using Langmuir and Freundlich isotherm models and its original equation and linearized form after integration[19-24].Langmuir isotherm: the monolayer coverage of the biosorption surface. This model assumes that biosorption occurs at specific homogeneous biosorption sites within the sorbent and intermolecular forces decrease rapidly with the distance from the biosorption surface [21-23]. The equilibrium relationship is described and its linearized form (Eq.(4)). The constants can be evaluated from the intercept (1/b.qm) and slope (1/qm) of the linear plot of C_e/q_e versus C_e. Freundlich isotherm: was originally empirical in nature but was later interpreted as sorption to heterogeneous surfaces or surfaces supporting sites of varied affinities. It is assumed that the stronger binding sites are occupied first and that binding strength decreases with the increasing degree of site occupation. Freundlich equation, which was applied for the biosorption of Th^{4+} ions, is given by Eq.(5) [22-24].The parameters are obtained from the slope (1/n) and the intercept (logk_F) of the plot of logq_e versus logC_e.

Langmuir equation (Eq.(4)):

$$q_e = \frac{q_m \times b \times C_e}{1 + b C_e} \qquad \text{Eq.(4a)}$$

After integration:

$$\frac{C_e}{q_e} = \frac{1}{b.q_m} + \frac{C_e}{q_m} \qquad \text{Eq. (4b)}$$

Freundlich equation (Eq.(5)):

$$q_{eq} = K_F C_e^{1/n} \qquad \text{Eq.(5a)}$$

After integration:

$$\log q_e = \log K_F + \frac{1}{n} \log c_e \qquad \text{Eq.(5b)}$$

Where, C_e is the equilibrium concentration (mg L^{-1}), q_e is the amount absorbed at equilibrium (mg g^{-1}), q_m is the maximum adsorption capacity of the sorbent (mg g^{-1}), b is the Langmuir isotherm constants (L mg^{-1}), K_f is the Freundlich isotherm constant, and n (dimensionless) is the heterogeneity factor.

Results & discussion

Synthesis of sorbent materials

A simple one-pot in situ co-precipitation method was used to synthesize functionalized magnetic-chitosan nanocomposites with iminodiphosphonic acid groups *via* three components one-pot synthesis. Fig. (1) shows the schematic route for the synthesis of α-aminophosphonic acid functionalized chitosan. In this reaction, methylene phosphonic groups are grafted on the chitosan moiety by reaction of phosphonic acid groups onto amine group in the

presence of formaldehyde, according to the general synthesis reaction (Fig. (2), assuming the mechanism of N-phosphonomethylation). The primary amine group (-NH$_2$) can be grafted by either one or two phosphonomethyl moiety for polysubstituted structure. Indeed, the final product may bear both mono-, and disubstituted amine e.g.: CS -NH-CH$_2$-PO(OH)$_2$ and/or CS –N(-CH$_2$- PO(OH)$_2$)$_2$ [20, 22].

Characterization of sorbents
Elemental analysis

The C, H, N, and P contents in the magnetic-chitosan nanocomposites (R-I) were 15.11($\pm$0.05)%, 2.75 ($\pm$0.13)%, 2.74 % ($\pm$0.03), and 0.0%, respectively. After methylene phosphonic groups are grafted the C, H, N, and P contents increased to 14.78($\pm$0.04)%, 3.21($\pm$0.03)%, 2.61% ($\pm$0.02), and 4.19% ($\pm$0.12), respectively. The P content (wt., %) in the polymer reaches 4.19% ($\pm$0.12)for R-II; this shows the efficient the phosphomethylation process (according to the synthesis scheme described on Fig. 1). The methylene phosphonic groups grafting on chitosan backbone logically reduces the C and N mass fractions in the R-II: the molecular weight of the final derivative strongly increases and then "dilute" C and N element in the final product [19-24].

FTIR Spectrometry

FTIR spectra were recorded at each step of the synthesis to confirm the successive changes in the structure of the biopolymer (Fig. (3)). Basically, the different spectra were very similar; the main differences were identified in terms of relative intensity. Several typical bands can be detected. The band at 568 cm^{-1} is assigned to Fe-O stretching vibration of Fe$_3$O$_4$ [19-21]. For the CS and MCS composite (a) a strong and broad band appears around 3299 cm^{-1}: this is generally attributed to the contributions of stretching vibration of–OH group, stretching vibration of N–H group and hydrogen bonds of polysaccharides. In the R-II (FMCS) spectrum brings new P-based reactive groups. This is confirmed by the appearance of typical bands at 746 cm^{-1}, assigned to υ(-P=O), at 932cm^{-1}, attributed to P-O-C stretching or to P-OH stretching [20, 24,26], at 1045cm^{-1}, associated to P-O-R bond and at 1244 cm^{-1}, assigned to P=O bond [23, 24]. These new peaks confirm the successful grafting of phosphorus-based reactive groups. Another characteristic peak of

primary amine–NH$_2$ appears at 1613 cm^{-1} (bending vibration). The bands at 1463 and 1364 cm^{-1} can be attributed to the C–O–C stretching or amide II and –OH bending vibrations, respectively [24]. The absorption band at 893 cm^{-1} corresponds to β-D-glucose unit [21]. The absorption bands around 1320 and 1065 cm^{-1} are generally assigned to the stretching vibrations of primary –OH group and secondary–OH group, respectively [21, 24].

Crystalline structure and X-ray diffraction pattern

The XRD patterns of raw chitosan (CS), R-I and R-II are displayed in Fig. (4). Here, raw substrate (CS) is characterized by 2 peaks corresponding to 2θ angles: 10.4°, 20.2° ((020, 110) diffraction planes, with plane distances close to 9.30Å and at 4.61Å respectively), that can be attributed to chitosan chain alignment controlled by intermolecular interactions. It is noteworthy that a small shoulder is also appearing at 2θ=23° [24]. Fig. 3 reports the XRD patterns of the R-I and R-II nanocomposite: the eight characteristic peaks of Fe$_3$O$_4$ are identified by their indices: (111), (220), (311), (400), (422), (511), (440), and (622). These peaks are consistent with the database in JCPDS file (PDF No. 65-3107): that is the representative of the cubic spinel structure of Fe$_3$O$_4$ [17, 19-21]. Using the highest intense peak corresponding to (311) index, the particles average diameter 30-40 nm using the Scherer equation.

pH$_{zpc}$

The pH-drift method was tested for different experimental concentrations (sorbent dosage, concentration of the background salt: 0.1 M NaCl solutions, contact time: 24 h); an example is given in Fig. (5). The pH$_{ZPC}$ of the different sorbents were obtained. The pH$_{ZPC}$ of raw chitosan was 8.52, which is consistent with the pKa value of 6.3–6.6 for the amino group in chitosan [24]. While magnetic-chitosan nanocomposite (MCS) has a pH$_{ZPC}$ close to 7.32; this was attributed to the decrease of –NH$_2$ content in magnetic-chitosan due to the incorporation of Fe$_3$O$_4$ nanoparticles (by one-third mass ratio). After amino-phosphomethylation, the pH$_{ZPC}$ of the sorbent drops to 4.50.This can be easily explained by the immobilization of phosphonic acid groups, where the α-aminophosphonic considered as a stronger diacid with pK$_{a1}$ 0.5–1.5 and pK$_{a2}$ 5–6 [20, 25].This is another proof that the chemical grafting is

efficiently operated on the biopolymer backbone to bring acidic functions. The significant decrease in the pH_{ZPC} confirms that high degree of the amine substitution which is attributed to the decrease of the electron density around nitrogen atom of amino groups due to withdrawing power of >P=O functionality [20].

TEM analysis

Nanocomposites morphological features were characterized by TEM. A typical low magnification TEM image of the nanoparticles obtained is shown in Fig. (6). The nanoparticles are relatively monodisperse [17], with an average size of 30-60 nm and with an average core size of 6-9 nm. The iron oxide (Fe_3O_4) nanoparticles tends to aggregate, probably due to dipole/dipole magnetic attraction [19-21].The contrast of the nanoparticles show a darker core surrounded by a lighter shell that reveals a core/shell structure. The dark areas represent crystalline Fe_3O_4, embedded into the bright ones are associated with organic framework polymer due to the different electron-absorbing abilities (i.e. the electron binding ability of Fe_3O_4 is higher than that of

the polymer shell) [20]. Therefore, the cores can be identified as the darker region compared to the shell area. High magnification of TEM shows the deep micrometric caves in the entire surfaces with irregular sizes with the intensive grafting of organic polymer.

Magnetic properties

Typical magnetization loops (hysteresis loop) (Fig. SI1: see supporting Information**)**, the absence of remanence and coercivity, prove that these nanocomposites are superparamagnetic materials [17, 20]. The saturation magnetization of R-I and R-II nanocomposites were about 34.92 and 21.15 emu g^{-1}, respectively; that easily recovered with the help of an external magnetic field. These values are much significantly lower than the bulk phase Fe_3O_4 magnetic nanoparticles (i.e., 92 emu g^{-1}). This decrease can be explained by several factors including experimental conditions used for the synthesis of magnetic particles, nanometric size effect, particle crystallization and the amount of magnetite embedded in diamagnetic polymer layer etc.. [17,19-21].
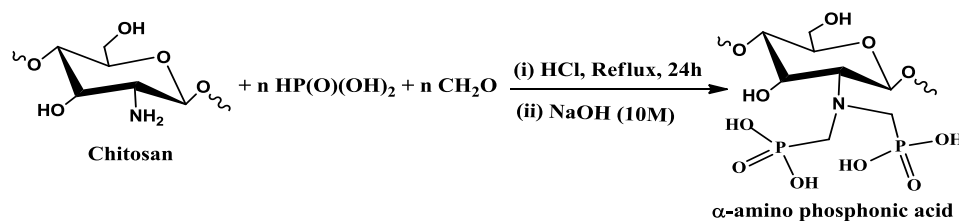
Fig. (1): Schematic route for one-pot synthesis of α-aminophosphonic acid functionalized chitosan.
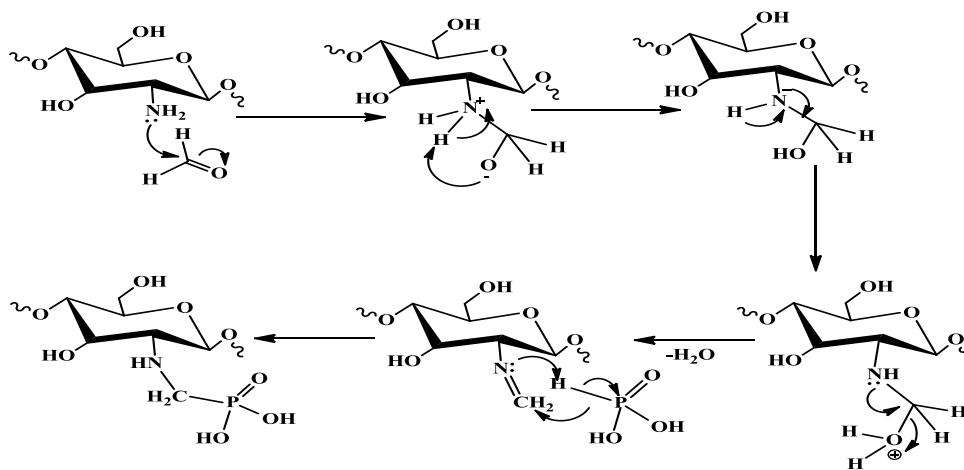
Fig. (2): Schematic for the N-phosphonomethylation of chitosan.
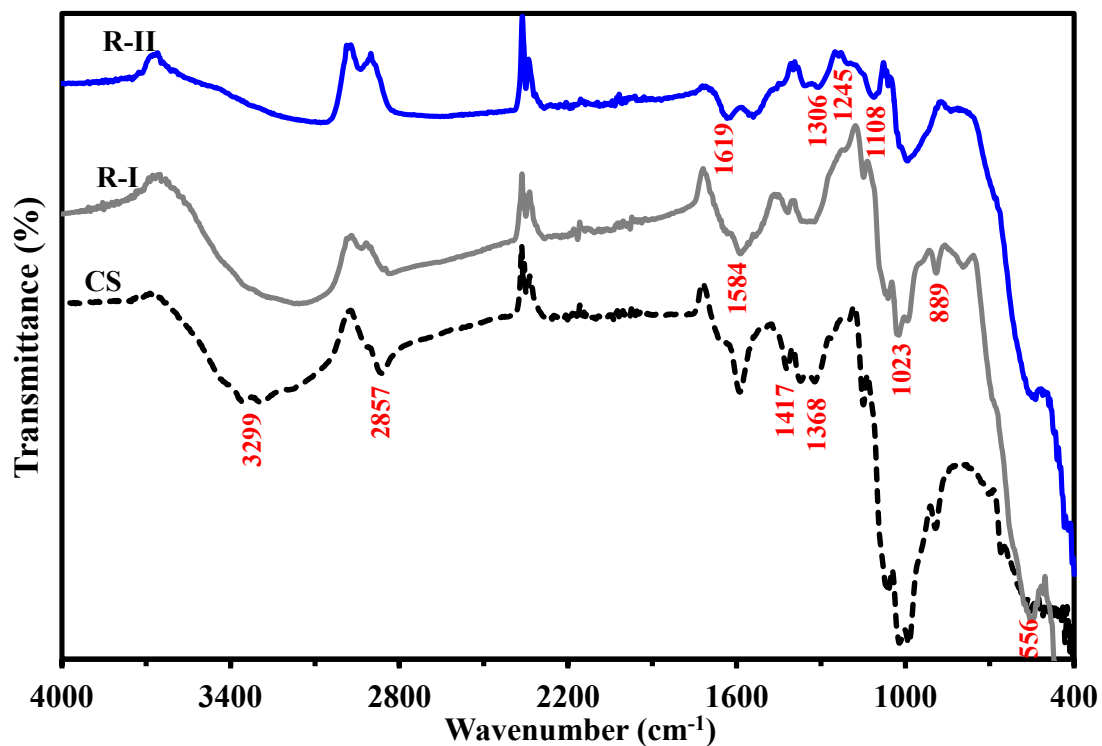
Fig. (3): FTIR spectra of chitosan (CS), magnetic-chitosan (R-I), and functionalized magnetic-chitosan (R-II) nanocomposites.
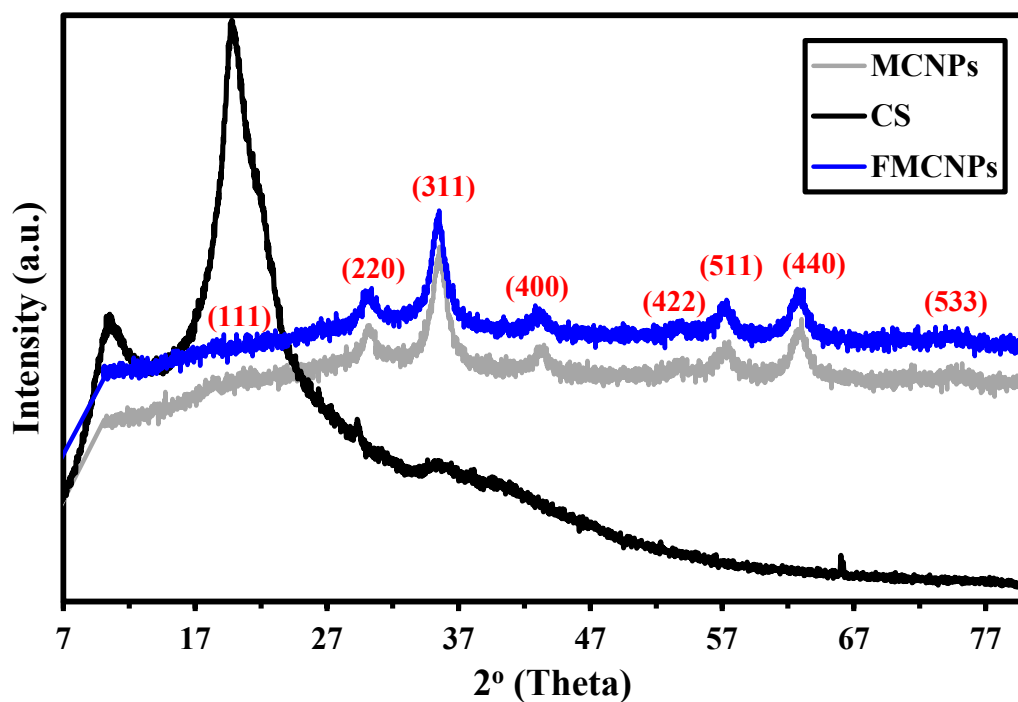
Fig. (4). XRD pattern of chitosan (CS), R-I (MCNPs), and R-II (FMCNPs) nanocomposites.
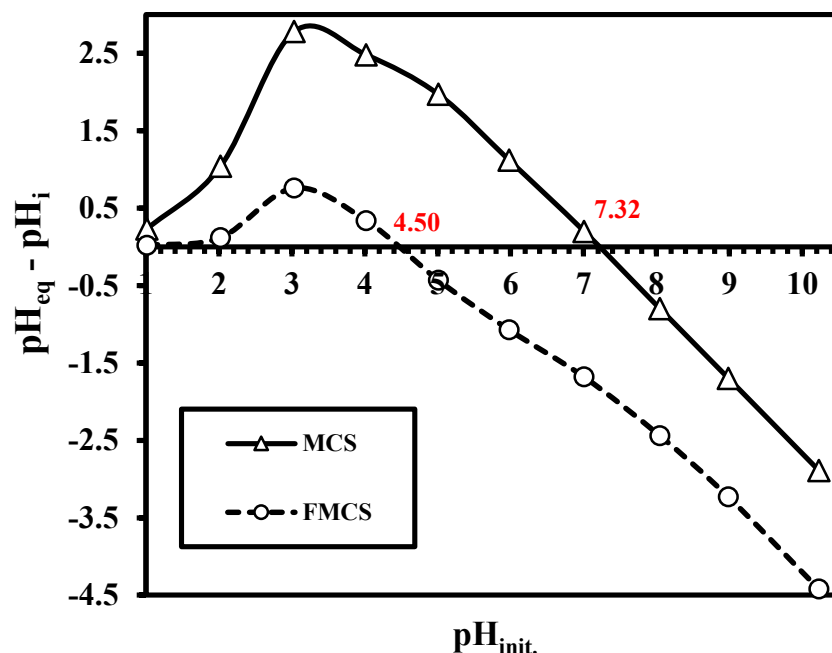
Fig. (5): Determination of pH$_{ZPC}$ for the sorbents by the pH-drift method–determination of the pH corresponding to pH$_i$ =pH$_{eq}$ (Example of test performed with sorbent dosage: 1g L^{-1}; Background salt: NaCl (0.1 M); agitation time: 24 h).
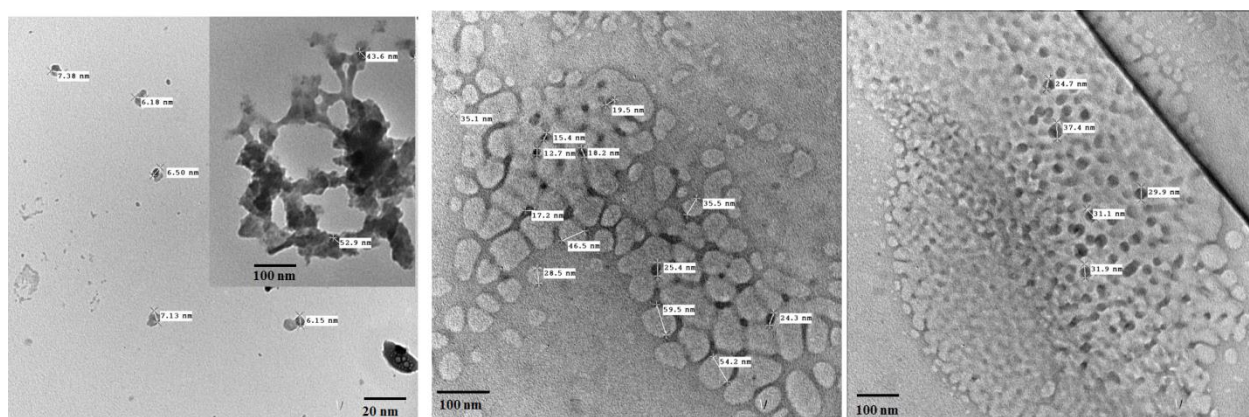
Fig. (6): TEM captures of the nanocomposite morphology (20 and 100 nm scale bar).

Sorption studies

Effect of pH and interpretation of sorption mechanisms

The pH may impact the surface properties of sorbent (protonation/deprotonation of reactive groups) and the speciation of metal species (formation of hydrolysed species or complexes). In the case of thorium metal ions in simple solutions cationic metal species may co-exist under different forms

(depending on pH and metal concentration). Fig. (7) compares the effect of pH$_{init.}$ on Th^{4+} sorption capacity for R-I and R-II, in the range 1.5-4.5. Above pH 6.0, the formation of hydrocolloids species causes a partial precipitation of thorium under the form of hydrolyzed species (i.e., Th(OH)$_4$); and at high concentration metal ions begin to precipitate[8].Th^{4+} exists in the form of Th(OH)$_3^+$ in acidic solutions (at pH < 3.0), and tend to form cationic hydrolyzed

species (such as $Th(OH)_2^{2+}$) at pH between 3.0 and 5.0 and when increasing the pH[8].In strong acidic solutions (pH < 3.5), both amino groups and phosphonate groups of the both sorbents are protonated, which results in positively charged surface of the sorbents. The competition of protons for binding on reactive sites and the repulsive effect of positively charged surface for Th^{4+} binding explain the dramatic decrease of sorption capacities [5, 21]. As the pH increases, the protonated amine and phosphonate groups gradually deprotonate. Therefore, the surface charge on the sorbents (carboxylate functions) turns negative, which significantly enhances the electrostatic interaction between the sorbent and metal cations [22, 24]. For these reasons, taking into account optimum efficiency, pH variation and both the stability of the sorbent and the speciation of metal ions, further experiments were performed at initial pH 3.5.

Different mechanisms may be involved in the binding of cationic species Th^{4+} in aqueous solution appear to be sorbed by combined chelation and anion-exchange mechanisms. Different effects may control the preference of Th^{4+} ions for the different sorbents R-I and R-II: (a) depending on the pH (in relation with the protonation/deprotonation of reactive groups and the speciation of Th^{4+} species, under selected experimental conditions), (b) the HSAB concept–Th^{4+} is considered a hard acid according Pearson's rules [13]; this means that the metal ion bind preferentially to ligands bearing N >> P, O >> S, and (c) The steric effect modulates the accessibility to reactive groups [26]. Actually, the effective binding mechanisms may be a contribution of these different mechanisms whose relative and respective importance depends on experimental conditions.

In the case of uranyl binding on magnetic polyglycidylmethacrylate functionalized with aminophosphonic groups, Galhoum et al. [19] reported the strong interaction of uranyl species with several functional groups (based on FTIR and XPS analysis). A tetradentate complex is formed by ionic bond with a deprotonated oxygen atom of phosphonate moiety, the coordinate bonding with 2 nitrogen donors of amine groups and the coordination with one oxygen donor of OH group. Actually, this binding may be affected by the pH through the speciation of Th^{4+}, but also the protonation/deprotonation of reactive groups, as reported above.

Effect of equilibration time and biosorption kinetic studies

Uptake kinetics for Th^{4+} ions were compared for the both sorbents (Fig. (7)). The curves, regardless sorbent type show similar trend. Initially, a very fast initial sorption (for the first 10 min) represents 49.0–64.0% of total sorption with an almost linear increase in sorption capacity (vs. time), (corresponding to a physisorption mechanism), and decreased slowly with increasing reaction time (i.e. followed by a chemical sorption involving charge neutralization, coordination, and chelation till equilibrium). After that, sorption rate was relatively nearly zero due to the attainment of the equilibrium [20, 23]. The sorption equilibria for the sorbents were achieved within 40.0 and 90.0 min. for R-II, and R-I, respectively, under selected experimental conditions. The change in the rate of Th^{4+} ions sorption depends mainly on the accessible sorption sites located at the surface of sorbent particles, the saturation degree of these active sites (e.g. amine, and phosphonic acid groups) and the sorption velocity is enhanced by the high concentration gradient between the solution, surface and the internal reactive sites [15, 20, 23]. By increasing sorption time, sorption velocity decreases due to a decrease in the concentration gradient and to the contribution of the mechanism of resistance to intraparticle diffusion [16, 17].At the end, the equilibrium plateau is systematically due to the availability of free active sites strongly decreased; where most of them being occupied, and approached saturation [15-17].

The kinetic profiles were modeled using the PFORE, the PSORE and the sRIDE (Fig. SI2). The experimental data have been fitted by the aforementioned kinetic models, and their specific parameters (together with their respective, R^2) are reported in Table (1). Experimental uptake kinetics was plotted after linearization using the different models (Fig. SI2). The calculated sorption capacity value PSORE clearly fits better experimental data (was consistent with the experimental one); the overestimated values by the PSORE model (the differences do not exceed 5.13–8.51%) than the

PFORE data (the overestimated differences do not exceed 8.47 –12.19 %), as shown in both Table (1)and Fig. SI2(see SI).Additionally, the correlation coefficient for the PSORE (R² >0.99) was much higher than in the case of the PFORE (R² > 0.97). The plot of q(t) vs. $t^{0.5}$ shows multi-linear plot (Fig. SI2, see SI) characterized by three main stages. The first two main stages, where one of them passes through the origin and the other does no pass. This indicates that the rate of sorption is affected by both intraparticle diffusion and boundary layer. At the third stage, the Th^{4+} sorption rate became zero due to sorption–desorption equilibrium [15-17].This section leads to the conclusion that uptake kinetics can be described by the PSORE. The chemisorption is the rate-controlling step that involves valence forces through sharing or exchange of electrons between the adsorbent surface and adsorbate ions. The resistances to film diffusion and intraparticle diffusion have a negligible effect on uptake kinetics [21].

Sorption isotherms

To evaluate sorbents capacities, thorium sorption isotherms were determined at pH 3.5 and 299 K (Fig. 7). Sorption capacity was increased with increasing the initial and equilibrium concentrations. Sorption curves are generally following the same trend by a number of successive steps including: (a) a sharp initial section with strongly increasing sorption capacity followed by (b) a progressive increase in the sorption capacity, and (c) terminated by a saturation plateau. As the initial Th^{4+} concentration gradually increases, and the driving force become more strongly, providing enough more energy between the solution and the active sorption sites [20, 23].The sorption progressively increases to reach a plateau close to maximum sorption capacities (q_{max}) reach 89.71 and 142.29 mg Th g^{-1} for R-I and R-II, respectively. This may be explained as the increase of Th^{4+} ions concentration, increases the number of competing ions for the available sorbents binding sites resulted in the limitation of vacant binding sites, which saturate beyond certain concentrations, thus decreasing Th^{4+} ions sorption efficiency [16, 21].

Fig. SI3 also shows the superimposition of experimental data with fitted curves using the equations of Langmuir, and Freundlich model. Different models parameters (with their determination coefficients, R^2) are summarized in Table (2). Adjustment quality can be evaluated by the value of R^2 and by comparison of the calculated and experimental values of equilibrium sorption capacities (Table (2)). Fig. SI3 shows the comparison of simulated curves for the Langmuir and Freundlich models. Obviously the Langmuir equation fits the experimental data much better than the Freundlich equation for which R^2 was systematically higher than 0.989 (compared to less than 0.916 for Freundlich), this was expectable based on the shape of sorption isotherms: the saturation plateau is consistent with the asymptotic trend associated to the Langmuir equation, while the Freundlich equation which is a power-like function [15-17, 22]. It is noteworthy that the modeled values for equilibrium sorption capacities (q_{eq}) were consistent with experimental observations and were systematically underestimated using the Freundlich (the differences about 78.6–89.1%) and overestimated by the Langmuir model (the differences do not exceed 4.9–9.3%). The simulated curve is close to experimental points as a confirmation of the suitability of the Langmuir equation to fit sorption isotherm. This suggests (to be verified by appropriate analytical procedures) that metal sorption occurs through monolayer uniform sorption, with a finite number of identical sites distributed over the sorbent surface [7, 15, 20].

For favorable analysis sorption properties, the value of a dimensionless constant (RL = $(1 + K_L C_o)^{-1}$): where K_L is the Langmuir constant and C_o is the initial metal concentration; must be lower than one [15, 21-24]. All RL values for the sorbent were lied between 0.07 and 0.44 for R-I and between 0.04 and 0.32 for R-II sorbent; all of them being smaller than 1, this means that thorium sorption on both sorbents is highly favorable, regardless of metal concentration.

Effect of temperature and thermodynamic studies

To study the effect of temperature on sorption of Th^{4+} ions, experiments were carried in the range 298-323 K. Thorium sorption increases with increasing the temperature (between 298 K and 323K, 25-50°C). Thermodynamics characteristic of thorium sorption at different temperatures were evaluated, based on the distribution coefficients K_d(L g^{-1}): the ratio of q_{eq}/C_{eq}, for each temperature, e.g. enthalpy change (ΔH^o), entropy change (ΔS^o) by the van't Hoff equation

$(\ln K_d = (\Delta H^o/R)1/T + \Delta S^o/R)$, while the free energy (ΔG^o) change can be deduced from $(\Delta G^o = \Delta H^o - T\Delta S^o)$ [19-21].

Fig. (7) shows the very similar trends obtained with these materials for which sorption capacity increases with temperature. Fig. (7) shows the linear plots of $\ln K_d$ vs. $1/T$, which allows determination of the thermodynamic parameters of the different systems (Table (3)) follow the same trends: (a) positive value of ΔH^o (very close for the both sorbents: ranging between 4.14 and 3.94 kJ mol^{-1}), indicating the endothermic nature of the sorption process. The global enthalpy changes consist of the combination of the dehydration enthalpy (ΔH_{dehydr}, which is supposed to be positive due to the energy required for breaking the ion–water and water–water bonding of the hydrated metal ions) and the complexation enthalpy ($\Delta H_{complex}$, also positive) [6], (b) positive value of ΔS^o (with values very close), indicating an increase in randomness after metal sorption (at the solid/liquid interface) and this may be due to the release of water molecules bound to metal ions or the exchange of metal ions with more mobile ions (initially present on the sorbent) [20, 22], (c) negative value of ΔG^o (the changes were of the same order of magnitude for both sorbents), indicating that the reaction is spontaneous (absolute value increases with temperature), and (d) the reaction is controlled by entropic changes than by enthalpy changes $(|\Delta H^o| < |T\Delta S^o|)$.

Table (1): Kinetics parameters for Th(IV) sorption.

Sorbent	PFORE		
	$K_1 \times 10^{-3}$, (min^{-1})	$Q_{eq.}$ (mg Th g^{-1})	R^2
R-I	51.13	45.58	0.961
R-II	70.70	67.44	0.972
Sorbent	PSORE		
	$K_2 \times 10^{-5}$, (mg g^{-1} min^{-1})	$Q_{eq.}$ (mg Th g^{-1})	R^2
R-I	231.773	52.36	0.996
R-II	306.383	83.33	0.998
Sorbent	sRIPD		
	$K_{id,1}$, (mg g^{-1} min$^{-0.5}$)	$K_{id,2}$, (mg g^{-1} min$^{-0.5}$)	$K_{id,3}$, (mg g^{-1} min$^{-0.5}$)
R-I	6.786	4.871	0.119
R-II	13.254	0.245	0.615

Table (2): Isotherms constants for Th(IV) sorption.

Sorbent	Langmuir isotherm model		
	$Q_{max.}$	K_L(L mg^{-1})	R^2
R-I	98.04	0.0479	0.9888
R-II	149.25	0.0984	0.9972
Sorbent	Freundlich isotherm model		
	n	K_F, (mg Th g^{-1})	R^2
R-I	2.36	10.666	0.9166
R-II	2.91	28.016	0.8515
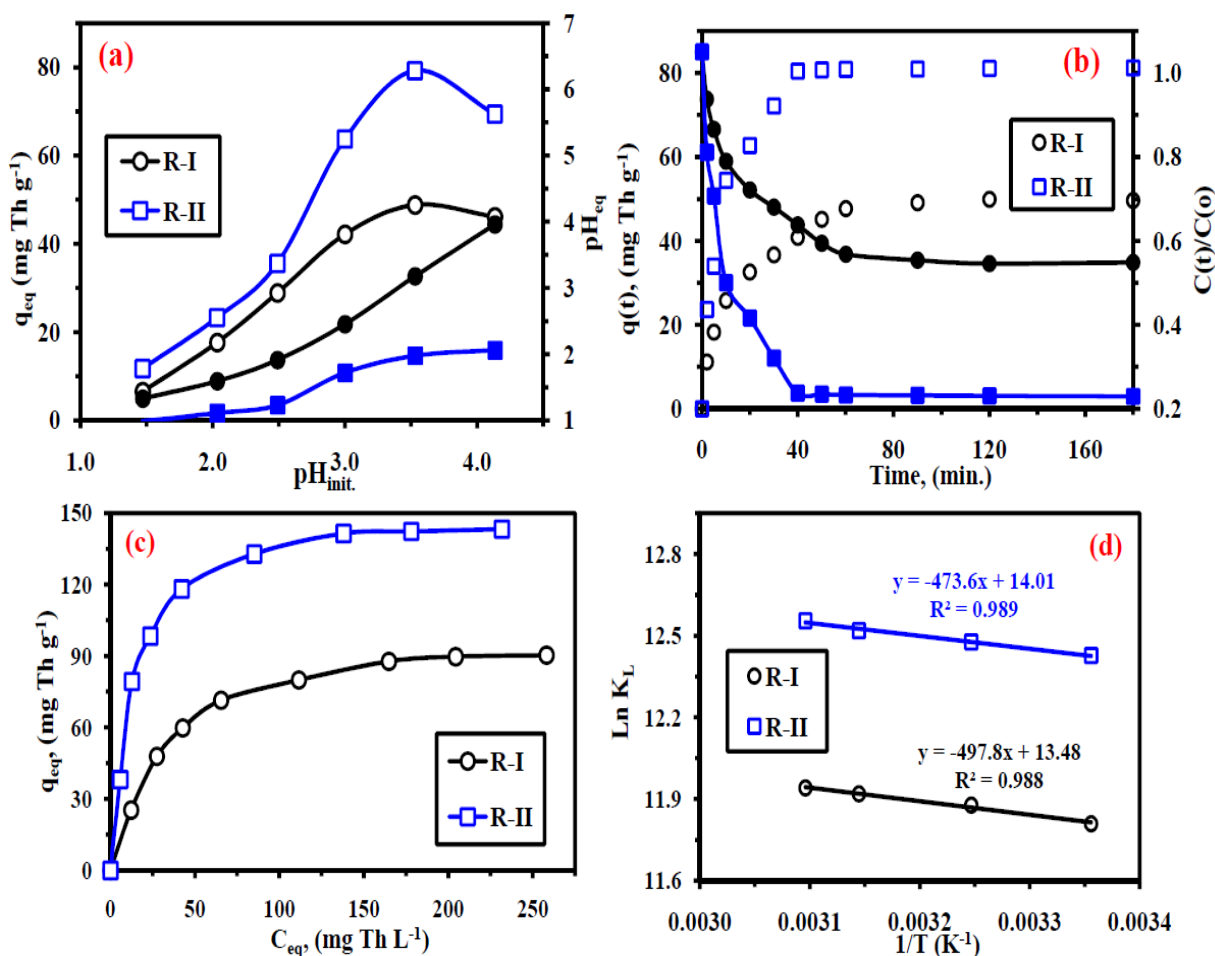
Fig. (7): (a) Effect of pH on Th^{4+} sorption: q_{eq} *vs* pH$_{init.}$ (open symbols) and pH$_{eq}$ *vs* pH$_{init.}$ (closed symbols). (C$_o$: 50 mg Th L^{-1}; T: 25 ^{o}C; SD: 0.5 g L^{-1}; Contact time: 3 h). (b) Effect of sorption time. (pH$_o$: 3.5; C$_o$: 50 mg Th L^{-1}; SD: 0.5 g L^{-1}; T: 25°C). (c) Effect of Th^{4+} concentration. (pH$_o$: 3.5; T: 25 ^{o}C; SD: 0.5 g L^{-1}; Contact time: 3 h). (d) Thermodynamics of Th^{4+} sorption using R-I and R-II nanocomposites–Van't Hoff plots of Ln KD *vs* 1/T. (pH$_o$: 3.5; C$_o$: 200 mg Th L^{-1}; SD: 0.5 g L^{-1}; Contact time: 1.5 h).

Table (3): Thermodynamic parameters of Th(IV) sorption.

Sorbent	Temp., K	ΔH^o (kJ/mol)	ΔS^o (J/mol)	ΔG^o (kJ/mol)	TΔS^o (KJ/mol)	R^2
R-I	298			-29.376	33.409	
	308	4.14	112.11	-30.490	34.530	0.9887
	318			-31.605	35.651	
	323			-32.162	36.212	
R-II	298			-30.310	34.723	
	308	3.94	116.52	-31.574	35.888	0.9892
	318			-32.748	37.053	
	323			-33.335	37.636	

Metal desorption and sorbent recycling

Sorbent reuse is a key step in the design of a sorption system. To reduce the cost of the removal process, regeneration of the resin should be carried out. The desorption of metal ions from loaded sorbents is generally performed using acidic solutions. In the present case, acidic conditions may cause the denaturation (dissolving and destruction) of the magnetic core of sorbent particles. It was necessary testing alternative eluents such as ethylenediamine tetraacetic acid (EDTA), thiourea and urea, which are known for being strong chelating agents for many metal ions. Two different eluents such as EDTA and urea (0.25 M) were used for Th^{4+} ions releasing. Table (4) shows that EDTA solution is more effective than urea, with efficiency more than 94 %. At the end of the first five cycles, the sorption and desorption efficiencies remain higher than 91% for a minimum of five sorption/desorption cycle, and is not significantly reduced. The nanocomposites sorbents have a good durability and stability in terms of sorption capacities. Actually, the very weak decrease in sorption/desorption performances contributes to confirm the stability of the material.

The distribution of the particle sizes of the different sorbents (analyzed by TEM) shows that the smallest particles can pass through the membranes. However, the side-aggregation (facilitated by the hydroxyl groups on the sorbents) may contribute to side aggregation that artificially grows the particle size while operating sorption. Actually, the weight loss at the first step was evaluated close to 3%, while it was negligible (below 1%) for the next cycles. This weak weight loss of sorbent can partially contribute to the slight decrease in sorption performance at sorbent recycling [26].

Comparison of sorption performance for Th^{4+} with various sorbents

Table (5) reports Th^{4+} sorption capacities of a series of different sorbents. Since the experimental conditions are not identical (e.g. sorbent dosage, time, pH, and solution composition), a direct comparison is not easy. These R-I and R-II sorbents have comparable in terms of two parameters (sorption capacities and uptake kinetics) to other sorbents, though some materials such as iron and aluminum oxide nanoparticles [3], single-layer GO [12], and PVA/SA/PEO/HZSM5 nanofiber [6] show very high remarkable sorption performance. However, the synthesized sorbents show higher efficiency than some other sorbents with polyaminated modified glycidyl methacrylate magnetic, [4], tin oxide NPs [10], PAN/zeolite composite [9], graphene oxide (GO) [11], and solidified Mannich type [5].

Table (4): Sorption (SE) and desorption (De) efficiencies cycles

Cycle no.	EDTA				Urea			
	R-I		R-II		R-I		R-II	
	De, (%)	SE, (%)	De, (%)	SE, (%)	De, (%)	SE, (%)	De, (%)	SE, (%)
1	93.59	100*	97.94	100*	88.17	100*	85.34	100*
2	92.55	93.34	96.44	97.68	81.89	86.22	81.19	89.26
3	88.69	89.97	94.42	95.07	79.40	81.75	74.86	86.68
4	84.54	87.72	92.78	93.70	72.45	74.64	72.02	81.10
5	82.08	85.20	91.62	92.41	68.81	70.25	70.02	75.08

* Reference value for metal ion sorption efficiency (at first cycle). (Eluent conc. (0.25M); T: 25 °C; SD: 0.5 g L^{-1}; time: 30 min)

Table (5): Comparison of sorption capacity for Th(IV) sorption with various sorbents.

Sorbent	pH	Time min.	q_{eq} mg Th g^{-1}	Temp. (K)	Eluent	Ref.
Fe-NPs	5.0	60	595.0	303	0.2 M HNO$_3$	[3]
Al-NPs	4.0	70	602.0			
Mag.-EDA@GMA/MBA	3.5	120	90.7	323	0.2 M HNO$_3$	[4]
Mag.-DETA@GMA/MBA		120	110.4			
PVA/SA/PEO/HZSM5 nanofiber	5.5	240	274.6	298	n.d.*	[6]
PMAA-g-Cel/Bent composite	5.0	180	188.1	303	0.1 M HNO$_3$	[7]
TMPGZDC	5.5	120	96.7	318	0.1 M HNO$_3$	[8]
PAN/zeolite composite	4.0	45	9.28	298	1M HCl	[9]
Solidified Mannich type	3.5	90	2.9	303	0.1 M HCl	[5]
Single-layer GO	3.0	120	410.8	299	0.1M H$_2$SO$_4$	[12]
Titanate nanotubes	3.0	480	232.6	328	n.d.*	[14]
Tin oxide NPs	6.0	180	62.5	288	n.d.*	[10]
graphene oxide (GO)	3.0	120	76.57	308	n.d.*	[11]
R-I (MCS nanocomposite)	3.5	90	89.70	298	0.25 EDTA	This work
PPA-PGMA	5.0	40	142.29	298	0.25 EDTA	This work

* n.d.: not mentioned in the paper.

Conclusions

A highly efficient nano-magnetic chitosan-based sorbents were prepared with super paramagnetic properties, characterized and investigated towards the Th^{4+} sorption. The uptake capacities were 89.7, 142.3 mg Th g^{-1} for R-I and R-II, respectively. The R-II sorbent exhibits good affinity for binding Th^{4+} ions. This is attributed to the chelating effect of aminomethylphosphonic acid group owing to the donor effect of nitrogen atom and electrostatic attraction of phosphonate group. For both sorbents, the kinetic and isotherm sorption data follow PSORE and Langmuir equation, respectively. Thermodynamic parameters obtained indicate that the sorption process is spontaneous with endothermic nature. Different mechanisms may be involved in the binding of cationic species Th^{4+} in aqueous solution appear to be sorbed by combined chelation and anion-exchange mechanisms. Finally, the sorbents can be regenerated with high efficiency using EDTA (0.25 mol L^{-1}) as the eluent; and the sorbent can be recycled for at least 5 sorption/desorption cycles.

References

1. T.P. Rao, P. Metilda, J.M. Gladis. Preconcentration techniques for uranium(VI) and thorium(IV) prior to analytical determination-an overview. Talanta, 68, 1047-64 (2006).

2. P.K. Vijayan, I.V. Dulera, P.D. Krishnani, K.K. Vaze, S. Basu, R.K. Sinha. Overview of the thorium programme in India. In: Revol JP, Bourquin M, Kadi

Y, Lillestol E, de Mestral JC, Samec K (eds) Thorium energy for the world. Springer, Cham (2016).

3. B.R. Broujeni, A. Nilchi, A. H. Hassani, R. Saberi. Comparative adsorption study of Th^{4+} from aqueous solution by hydrothermally synthesized iron and aluminum oxide nanoparticles. Int. J. Enviro. Sci. Techno., 16, 4069 - 4082 (2019).

4. M.O. Abd El-Magied, E.A. Elshehy, E.A. Manaa, A.A. Tolba, A.A. Atia. Kinetics and thermodynamics studies on the recovery of thorium ions using amino resins with magnetic properties. Ind. Eng. Chem. Res., 55, 11338-11345 (2016).

5. A.R. Elsalamouny, O.A. Desouky, S.A. Mohamed, A.A. Galhoum: Evaluation of adsorption behavior for U(VI) and Th(IV) ions onto solidified Mannich type material. J. Disper. Sci. Technol., 38,360-365 (2017).

6. M. Talebi, S. Abbasizadeh, A.R. Keshtkar. Evaluation of single and simultaneous thorium and uranium sorption from water systems by an electrospun PVA/SA/PEO/HZSM5 nanofiber. Process Saf Environ, 109, 340-356, (2017).

7. T. S. Anirudhan, P. S. Suchithra, P. Senan, A. R. Tharun. Kinetic and equilibrium profiles of adsorptive recovery of thorium(IV) from aqueous solutions using poly(methacrylic acid) grafted cellulose/bentonite superabsorbent composite. Ind. Eng. Chem. Res., 51, 4825−4836 (2012).

8. T.S. Anirudhan, S.R. Rejeena. Thorium(IV) removal and recovery from aqueous solutions using tannin-modified poly(glycidylmethacrylate)-grafted zirconium oxide densified cellulose. Ind. Eng. Chem. Res., 50, 13288–13298 (2011).

9. A.K. Kaygun, S. Akyil. Study of the behavior of thorium adsorption on PAN/zeolite composite adsorbent. J. Hazard. Mate., 147, 357–362 (2007).

10. A. Nilchi, T.S. Dehaghan, S.R. Garmarodi. Kinetics, isotherm and thermodynamics for uranium and thorium ions adsorption from aqueous solutions by crystalline tin oxide nanoparticles. Desalination 321, 67–71 (2013).

11. D. Jiang, L. Liu, N. Pan, F. Yang, S. Li, R. Wang, I.W. Wyman, Y. Jin, C. Xia. The Separation of Th(IV)/U(VI) via selective complexation with graphene oxide. Chem. Eng. J., 271,147-154. (2015).

12. N. Pan, D. Guan, T. He, R. Wang, I. Wyman, Y. Jin, C. Xia. Removal of Th4+ ions from aqueous solutions by graphene oxide. J. Radioanal. Nucl. Chem., 298, 1999–2008 (2013).

13. R.G. Pearson Acids and bases. Science 151 (3707)172–177 (1966).

14. J. Liu, M. Luo, Z. Yuan, A. Ping. Synthesis, characterization, and application of titanate nanotubes for Th(IV) adsorption. J. Radioanal. Nucl. Chem. 298, 1427–1434 (2013).

15. H. Qiu, L. Lv, B. Pan, Q. Zhang, W. Zhang, Q. Zhang. Review: critical review in adsorption kinetic models. J Zhejiang Univ. Sci. A., 10,716–724 (2009).

16. M.N. El-Bohy, Y.K. Abdel-Monem, K.A. Rabie, N.M. Farag, M.G. Mahfouz, A.A. Galhoum, E. Guibal. Grafting of arginine and glutamic acid onto cellulose for enhanced uranyl sorption. Cellulose, 24, 1427-1443 (2017).

17. A.A. Galhoum, M.G. Mahfouz, N.A. Gomaa, T. Vincent, E. Guibal. Chemical modifications of chitosan nano-based magnetic particles for enhanced uranyl sorption. Hydrometallurgy, 168, 127–134 (2017).

18. Z. Marczenko. Separation and Spectrophotometric Determination of Elements, 2nd. Ed. Ellis Horwood, Chichester, UK (1986).

19. A.A. Galhoum, W.H. Eisa, I.E. El-Sayed, A.A. Tolba, Z.A. Shalaby, S.I. Mohamady, S.S. Muhammad, S.S. Hussin, T. Akashi, E. Guibal. A new route for manufacturing poly(amino-phosphonic)-functionalized poly(glycidyl methacrylate)-magnetic nanocomposites - Application to uranium sorption. Environ. Pollut., 264, 114797-114812 (2020).

20. A.A. Galhoum. Facile synthesis of functionalized polyglycidyl methacrylate-magnetic nanocomposites for enhanced uranium sorption. RSC Adv., 9, 38783-38796 (2019).

21. A.A. Galhoum, M.G. Mahfouz, N.A. Gomaa, S.S. Abdel-Rehem, A.A. Atia, T. Vincent, E. Guibal. Cysteine-functionalized chitosan magnetic nanobased particles for the recovery of uranium(VI): uptake kinetics and sorption isotherms. Sep. Sci. Techno., 50, 2776–2789 (2015).

22. A.A. Tolba, S.I. Mohamady, S.S. Hussin, T. Akashi, Y. Sakai, A.A. Galhoum, E. Guibal. Synthesis and characterization of poly(carboxymethyl)-cellulose for enhanced La(III) sorption Carbohyd. Polym., 157,1809–1820 (2017).

23. A.A. Galhoum, E.A. Elshehy, D.A. Tolan, A.M. El-Nahas, T. Taketsugu, K. Nishikiori, T. Akashi, A.S. Morshedy, E. Guibal. Synthesis of polyaminophosphonic acid-functionalized poly(glycidyl methacrylate) for the efficient sorption

of La(III) and Y(III). Chem. Eng. J., 375, 121932-121948 (2019).

24. E.A. Imam, I.E. El-Sayed, M.G. Mahfouz, A.A. Tolba,T. Akashi, A.A. Galhoum, E. Guibal. Synthesis of α-aminophosphonate functionalized chitosan sorbents: Effect of methylvsphenyl group on uranium sorption. Chem. Eng. J., 352, 1022–1034 (2018).

25. J. Viveros-Ceballos, M. Ordóñez, F. Sayago, C.

Cativiela. Stereoselective synthesis of α-amino-C-phosphinic acids and derivatives. Molecules, 21, 1141–1170 (2016).

26. M.M. Rashad, I.E. El-Sayed, A.A. Galhoum, M.M. Abdeen, H.I. Mira, E.A. Elshehy, S.g. Zhang, L. Xingmei, J. Xin, E. Guibal. Synthesis of α-aminophosphonate based sorbents – Influence of inserted groups (carboxylic vs. amine) on uranyl sorption. Chem. Eng. J., (2020) 127830. (in press).

تفعيل تراكيب الكايتوسان النانومتريه ذات الصفات المغناطيسيه لتعزيز إمتزاز أيونات الثوريوم الرباعي (Th^{IV})

لقد اصبح تصميم مواد ممتزه مخلبيه جديده فعاله لإمتزاز أيونات الثوريوم الرباعي تحدي لكثير من الباحثين , هذه الدراسه تصف طريقة تحضير بسيطه من خطوه واحده باستخدام طريقة الترسيب المصاحب تم تطبيقها لتخليق تراكيب الكايتوسان النانومتريه ذات الصفات المغناطيسيه والحامله لمجموعات وظيفيه متعدده لتعزيز إمتزاز أيونات الثوريوم الرباعي من المحاليل المائيه. تم توصيف التراكيب النانومتريه التي تم تحضيرهاعن طريق دراسة الخصائص الكيميائيه والفيزيائيه لها باستخدام الطرق الطيفية والتحليلية المختلفة مثل التحليل العنصرى للمواد والتحليل الطيفي للأشعة تحت الحمراء لإثبات تركيب المواد الناتجة والماسح الالكترونى المجهرى وكذلك تحليل الأشعة السينية بالاضافه تحليل مقياس المغناطيسية. تم دراسة السلوك الإمتزازي لهذه التراكيب المغناطيسيه (R-I) قبل وكذلك بعد عملية التفعيل والتنشيط (R-II) من خلال دراسة العوامل المؤثره على عملية الإمتزاز كما تم معالجة النتائج التي تم الحصول عليها من اجل حساب المعاملات الحركيه والحراريه بالإضافه الى دراسة عملية استرجاع العنصر بعد الفصل وعملية اعادة تنشيط الماده الممتزه للإستخدام المتكرر. و قد اوضحت النتائج ان حجم التراكيب النانومتريه هو 25,0 نانومتر كما أوضحت النتائج ان تطعيم التراكيب المغناطيسيه بمجموعات المثيلين فوسفونك أدى إلى زيادة كفاءة عملية الامتزاز بشكل كبير حيث بلغة سعة التشبع 89,7 و 142,3 ملليجرام من الثوريوم الى كل جرام من الماده الممتزه (R-I) و (R-II) على الترتيب وذلك عند الرقم الهيدروجيني 5.3 . كما أظهرت النتائج أن عمليه الامتزاز تلقائيه وماصه للحراره وتخضع الى التغير في العشوائيه اكثر من التغير في المحتوى الحراري وتتبع التفاعل من الرتبه الثانيه كما يمكن وصف عملية الامتزاز باستخدام نموذج لانجمير. تم استعادة ايونات الثوريوم بكفاءة باستخدام محلول (EDTA) بتركيز 0,25 مولر كما انه يمكن استخدام التراكيب المغناطيسيه لفصل واسترجاع أيونات الثوريوم بكفاءة بشكل متكرر لعدد خمس دورات على الاقل من الامتزاز والاسترجاع.